Plasmonic Nanohole Sensor for Capturing Single Virus-Like Particles toward Virucidal Drug Evaluation

*Joshua A. Jackman, Eric Linardy, Daehan Yoo, Jeongeun Seo, Wei Beng Ng, Daniel J. Klemme, Nathan J. Wittenberg, Sang-Hyun Oh, and Nam-Joon Cho**

Viruses, exosomes, and other microvesicles exemplify the rich diversity of nanoscale, phospholipid membrane-enclosed particulates which are found in nature.[1,2] The aforementioned biological materials hold broad clinical significance as the culprits and markers of numerous medical illnesses.[3] Of particular interest are enveloped viruses, which are a leading cause of worldwide morbidity and mortality and include the HIV, influenza, and dengue viruses among many more. There is enormous interest in the development of molecular detection and characterization tools for viral infection diagnosis as well as for antiviral drug evaluation.[4] Indeed, the emergence of drug-resistant virus strains is a growing problem and new classes of antiviral drugs are urgently needed.[5] Conventional methods for virus evaluation and pharmaceutical drug analysis focus on cell infectivity readouts whereby a drug is evaluated on the basis of treating or preventing virus infection.[6] Because almost all antiviral drugs on the market inhibit viral genome replication or boost the host cell immune response, the conventional methods have generally proven sufficient for antiviral drug evaluation.[7] However, there are important shortcomings, including long incubation times and difficulties to establish efficient cell culture models for certain viruses.[8] Surface-based measurement platforms offer a promising alternative in order to directly monitor the interactions between virus particles and drug candidates.[9] Such capabilities would bypass the requirement for cell culture models, provide a rapid, label-free readout, and also aid the development of the emerging class of virucidal agents which inactivate virus particles. Virus analytes are typically present in low concentrations, which further motivates the development of highly sensitive and selective platforms.

Nanoplasmonic sensors based on metallic nanoparticles or nanoholes demonstrate significant potential to address this capability gap.[10–13] When incident light excites conduction band electrons in a metallic nanostructure, a surface plasmon resonance (SPR) can be generated which gives rise to tightly confined optical fields that can be utilized in biosensing.[14] Sensing benefits include short and tunable evanescent field decay length, high sensitivity, and simple optical configuration.[15] Among different nanostructures, periodic nanohole arrays exhibit particularly intense resonances at specific wavelengths based on extraordinary optical transmission.[16] Depending on the array dimensions (e.g., nanohole shape, size, and periodicity), there are a series of extinction maximums (suppressed transmission) and minimums (enhanced transmission) associated with different plasmon modes.[17] If an analyte binds to the surface of the plasmonic nanostructure, then there will be a spectral shift due to changes in the local refractive index, and this shift can be tracked by monitoring transmission peaks[18] or the minimum.[19] There has been extensive development of nanohole SPR applications for molecular binding analysis, including biotin-streptavidin,[20] antibody-lipid,[21] DNA hybridization,[22] membrane protein,[23] and protein-glycan[24,25] interactions as well as protein biomarker detection.[25] Extending this line of work, detection of viruses and exosomes has also been reported. Yanik et al. introduced a protocol to detect viruses in biological media based on virus binding to antibody-functionalized porous nanoholes.[26] Im et al. recently demonstrated the molecular profiling of exosomes by measuring the binding of exosomes to a multiplexed nanohole array functionalized with different antibody markers.[27] So far, biosensing applications for periodic nanohole arrays have strictly focused on binding detection, and other biosensing possibilities such as analysis of conformational changes[28] and structural transformations[29] remain to be explored. Taking into account the high sensitivity of the periodic nanohole array along with versatile sensing possibilities (e.g., flow-through configuration,[30–33] high-throughput measurements,[34,35] and compatibility with other surface-sensitive measurement techniques[36]), there is compelling motivation to explore new

J. A. Jackman, E. Linardy, Dr. J. Seo, W. B. Ng, Prof. N.-J. Cho
School of Materials Science and Engineering
Nanyang Technological University
50 Nanyang Avenue, 639798, Singapore
E-mail: njcho@ntu.edu.sg

J. A. Jackman, E. Linardy, Dr. J. Seo, W. B. Ng, Prof. N.-J. Cho
Centre for Biomimetic Sensor Science
Nanyang Technological University
50 Nanyang Drive, 637553, Singapore

D. Yoo, D. J. Klemme, Prof. N. J. Wittenberg, Prof. S.-H. Oh
Department of Electrical and Computer Engineering
University of Minnesota
200 Union Street SE, Minneapolis, MN 55455, USA

Prof. N.-J. Cho
School of Chemical and Biomedical Engineering
Nanyang Technological University
62 Nanyang Drive, 637459, Singapore

DOI: 10.1002/smll.201501914

applications for periodic nanohole arrays, especially in the context of virucidal drug evaluation.

The goal of this study is to develop a plasmonic nanohole sensor for capturing virus-like particles and evaluating virucidal drug candidates. To initiate the study, the size distribution of dengue virus particles before and after treatment with a virucidal drug candidate was measured by nanoparticle tracking analysis. Based on the measured virus size distribution, a periodic nanohole array platform was fabricated with suitable nanohole dimensions (e.g., diameter, height) to host viruses and virus-like particles. A surface functionalization strategy was utilized in order to passively and selectively immobilize cholesterol-enriched model virus particles only inside the nanoholes, and not in the space between the nanoholes. Scanning electron microscopy (SEM) verified that single particles were immobilized only within the functionalized nanoholes. Based on this platform, a series of nanohole-based SPR biosensing experiments were conducted which demonstrate that a low surface coverage of particles only inside the functionalized nanoholes significantly improves nanoplasmonic sensing performance over nonfunctionalized nanoholes. The sensing approach enables highly sensitive and specific detection of virucidal peptide-induced particle rupture. Spectral analysis of the three measured transmission peaks further gives insight into the measurement sensitivity of the various plasmon modes. In addition, the findings outline a new method to functionalize the sidewalls of gold nanoholes with supported lipid bilayer membranes.

Our study is inspired by the virucidal activity of an amphipathic, α-helical (AH) peptide which is known to rupture lipid vesicles and exhibits virucidal activity against many kinds of enveloped viruses[37–39] (**Scheme 1**). Due to the increasing resistance of many medically important viruses to conventional antiviral drugs, the AH peptide is an attractive drug candidate with a novel mechanism of action based on lipid membrane solubilization.[40] Importantly, the lipid envelope surrounding certain viruses is derived from human cell membranes and not encoded in the mutation-prone viral genome. Hence, the lipid envelope is an attractive drug target because there is a very high barrier to the emergence of drug-resistant virus strains.[41] The AH peptide also preferentially targets highly curved membranes with nanometer-scale radii of curvature, offering a basis for therapeutic selectivity against viruses.[37] In order to define a suitable geometry for the nanohole sensor platform, we first characterize dengue virus particles (type 2, New Guinea C strain) using nanoparticle tracking analysis.[42] Optical images visualize the elastic scattering of individual virus particles in solution and demonstrate that AH peptide treatment causes the dissolution of virus particles. It was determined that the virus particles are initially around 137 nm diameter. After treatment with AH peptide at 37 °C for 1 h, virus particle degradation due to the lipid–peptide interaction was observed leading to the formation of approximately 50 nm particles, with a marked reduction in the measured particle concentration. Based on these observations, we designed a periodic

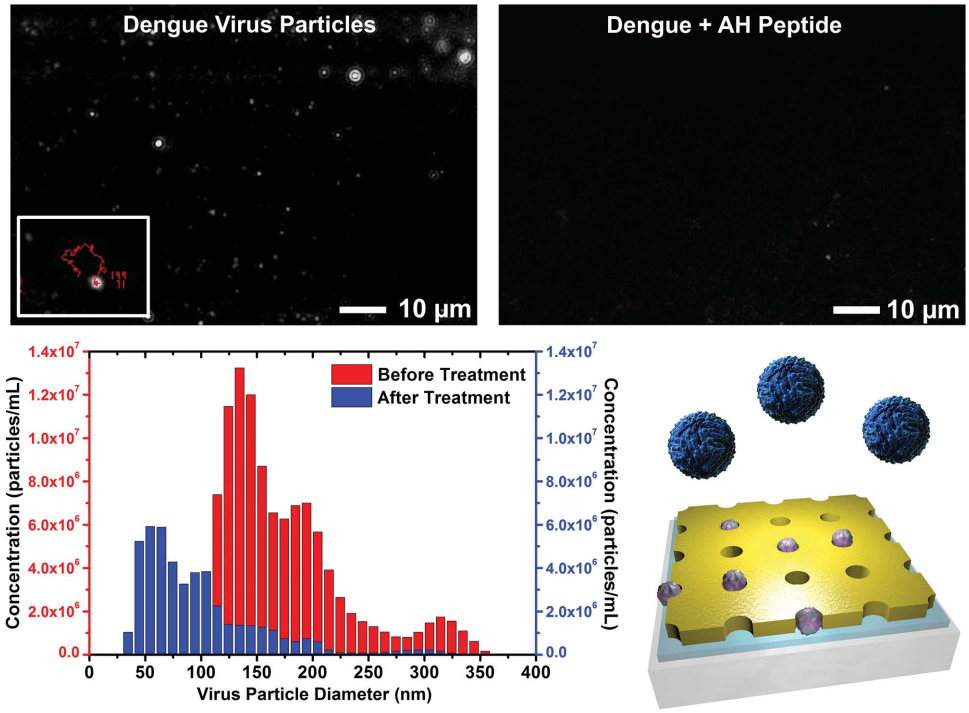

Scheme 1. Rupture of dengue virus particles by AH peptide. (Top) Optical micrographs (20×) obtained with nanoparticle tracking analysis visualize the elastic light scattering caused by individual dengue virus particles in solution. Inset shows the tracking assignment of an individual virus particle. Upon AH peptide treatment, there is a marked decrease in the size and number concentration of nanoscale particulates. Note that the two micrographs were obtained under the same intensity gain. (Bottom, left) Quantitative particle size and concentration measurements of dengue virus particles before (red) and after (blue) treatment with 26 μM AH peptide. (Bottom, right) Schematic of periodic gold nanohole array which was designed in order to selectively capture lipid vesicles and virus particles inside the nanoholes. The 1 × 1 cm gold nanohole array was formed on a glass substrate by the template-stripping method, and there is an optical adhesive layer between the gold and glass.

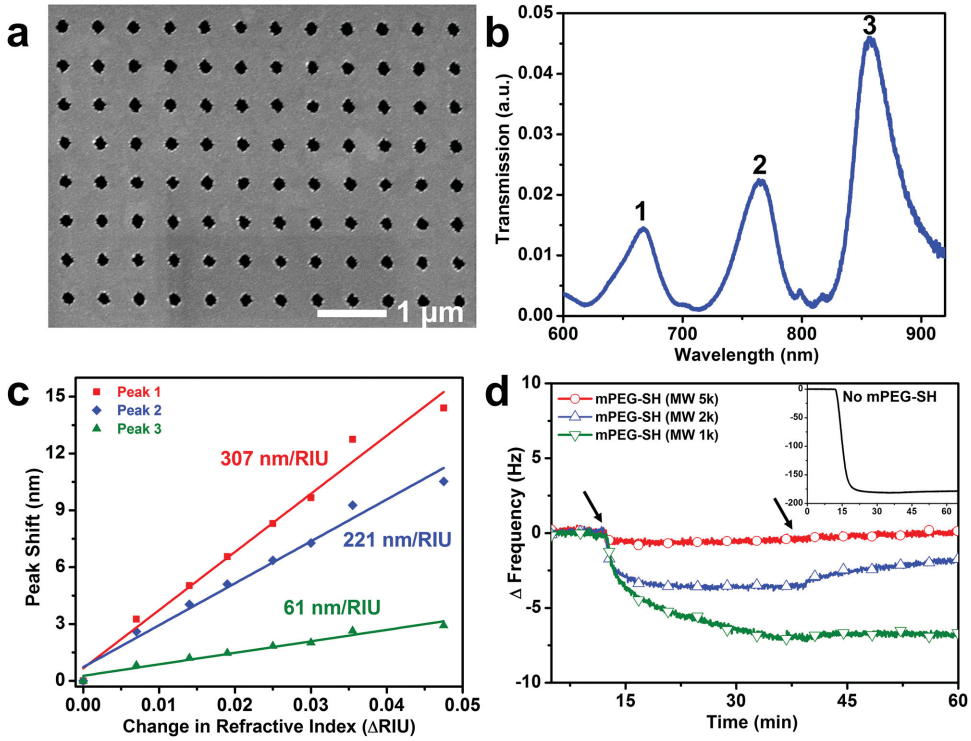

Figure 1. Development of plasmonic nanohole sensor platform. a) SEM image of nonfunctionalized periodic gold nanohole array obtained at 20 000× magnification. b) Optical transmission spectra of the gold nanohole array in aqueous buffer solution (10 mM Tris [pH 7.5] with 150 mM NaCl). The three transmission peaks are labeled as Peaks 1, 2, and 3, respectively. c) Spectral shift of the three transmission peaks measured in a series of water-glycerol mixtures (0 to 35 wt% glycerol). The bulk refractive index sensitivity (nm RIU^{-1}) of each transmission peak was obtained by calculating the slope of the corresponding linear fit. d) QCM-D frequency shift experiments were performed in order to measure virus-like particle adsorption onto mPEG-SH-functionalized gold surfaces. Surfaces were precoated with 1, 2, or 5 kDa mPEG-SH. The baseline signal was recorded in aqueous buffer solution, followed by 0.3 mg mL^{-1} virus-like particle addition at $t = 15$ min (see arrow). A buffer rinse was performed around $t = 40$ min (see arrow). Inset shows a control experiment that was similarly performed on a nonfunctionalized gold surface without mPEG-SH.

nanohole array with appropriate size dimensions in order to selectively immobilize single virus particles inside the nanoholes. This approach enables functional analysis of virus particles, including interactions with antibodies and virucidal agents. Here, we focus on the development of the plasmonic nanohole sensor platform with cholesterol-enriched model virus particles[43,44] in order to evaluate the virucidal activity of the AH peptide drug candidate.

Figure 1a presents an SEM image of a periodic gold nanohole array with 160 nm hole diameter and 500 nm periodicity template-stripped using optical adhesive (Norland, NOA 61) and a glass substrate.[45,46] The nanohole diameter and array periodicity are suitable for efficient coupling to plasmon modes at visible wavelengths.[15] The top surface and sidewalls of the holes are gold while the bottom surface is cured optical adhesive. For nanohole SPR sensing, the periodic nanohole array is illuminated with a tungsten-halogen lamp and the transmitted light from the periodic nanohole array is collected by an optical fiber and sent to the spectrometer. The optical transmission spectrum of the nanohole array covered with aqueous buffer solution shows complex features, including multiple transmission maxima and minima (Figure 1b). Because the experimental strategy is based on particle immobilization within the nanoholes, spectral analysis focused on the transmission peaks which are expected to be more sensitive to local refractive index changes inside the nanoholes.[17] In the measured wavelength range, three transmission peaks are observed and located around 680, 745, and 850 nm, respectively. These peaks are identified as (1,1) at the Au–epoxy interface, (1,0) at the Au–water interface, and (1,0) resonance at the Au–epoxy interface, respectively, where the integers represent the Bragg resonance orders.[47] The exact positions of these peaks are highly sensitive to the local refractive index environment[48] and time-resolved measurements which follow the peak positions can monitor the kinetics of interfacial adsorption processes. In order to determine the bulk refractive index sensitivity of each transmission peak, optical transmission measurements were recorded in various index-calibrated water–glycerol mixtures (0–35 wt% glycerol). With increasing refractive index, all three transmission peaks shift toward longer wavelengths (Figure 1c). The peak around 680 nm has the greatest bulk sensitivity (Peak 1: 307 nm RIU^{-1}), followed by the peak around 745 nm (Peak 2: 221 nm RIU^{-1}) and lastly the peak around 850 nm (Peak 3: 61 nm RIU^{-1}). Based on the measurement configuration,[36] the minimum refractive index resolution was determined to be 5.5×10^{-5} RIU by taking into account the spectral noise over a 1 min measurement period (1.68×10^{-2} nm) and the bulk sensitivity associated with Peak 1.

Surface functionalization of the gold nanohole array was then performed in order to selectively immobilize the virus-like particles inside the nanoholes. The gold

www.MaterialsViews.com

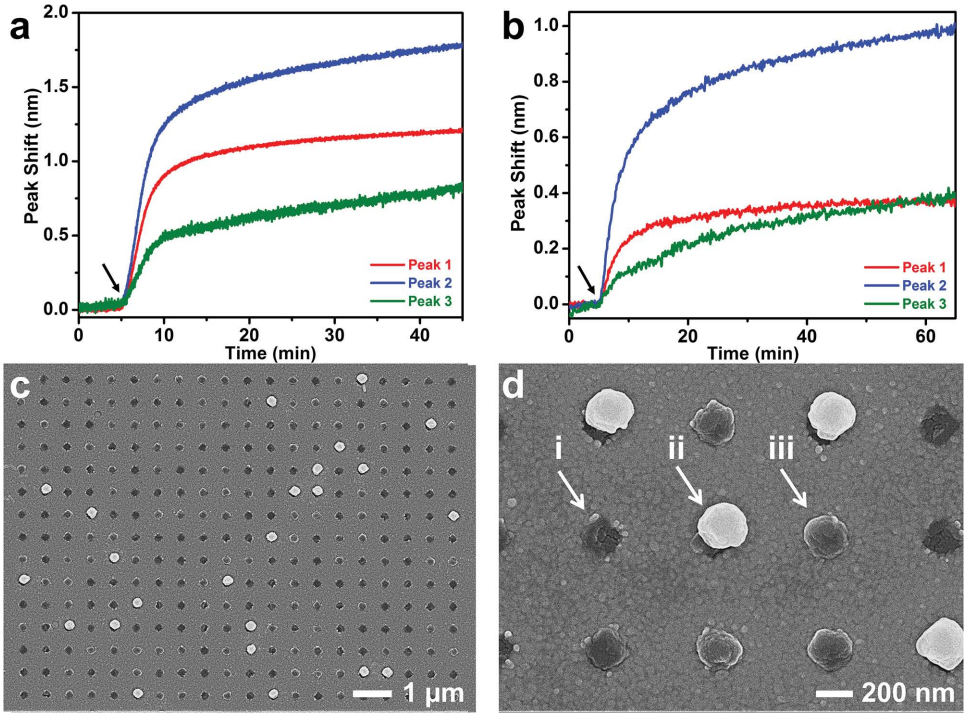

Figure 2. Selective adsorption of virus-like particles into functionalized nanoholes. Nanohole SPR experiments were performed on a) nonfunctionalized and b) mPEG-SH-functionalized nanohole arrays. Spectral shifts as a function of time were recorded for all three transmission peaks. The baseline signal corresponds to aqueous buffer solution. Then, 0.3 mg mL^{-1} virus-like particles were added (denoted by arrow) and the particle rupture process was tracked. SEM images obtained at c) 20000× and d) 40 000× magnification demonstrate that single virus-like particles adsorbed into individual nanoholes on the mPEG-SH-functionalized nanohole array. In part (d), arrows indicate the three cases: (i) no particle in the nanohole; (ii) one particle partially inside the nanohole; and (iii) one particle predominately inside the nanohole. Aside from the nanohole positions, nonspecific adsorption of virus-like particles was not observed on the mPEG-SH-functionalized gold surface.

surface was functionalized with thiol-terminated methoxy polyethylene(glycol) (mPEG-SH), which is known to confer fouling resistant properties.[49] The goal of this surface functionalization scheme was to block particle adsorption on the top surface between gold nanoholes as well as on the sidewalls of nanoholes, thereby allowing vesicle adsorption only inside the nanoholes. This scheme contrasts with that recently reported by Im et al., which instead focused on surface functionalization of the gold surface with antibody-conjugated PEG chains in order to capture exosomes on the nanohole sidewalls and on top of the gold surface.[27] To identify the optimal mPEG-SH chain length for minimal virus-like particle adsorption, quartz crystal microbalance-dissipation (QCM-D) experiments were conducted on gold-coated substrates (Figure 1d). Each substrate was functionalized with 1k, 2k, or 5k Da mPEG-SH chains. A baseline measurement signal was recorded in aqueous buffer solution and then addition of the virus-like particles was initiated at $t = 10$ min under continuous flow conditions. The virus-like particles had approximately 75 nm diameter, and the particle composition was 70 mol% 1,2-dioleoyl-*sn*-glycero-3-phosphocholine lipid and 30 mol% cholesterol. Upon particle adsorption onto the substrate, there was a decrease in the resonance frequency which is negatively proportional to the amount of adsorbed mass.[50] At $t = 40$ min, a buffer washing step was performed in order to remove weakly bound adsorbate. As a control experiment, virus-like particle adsorption on a bare gold substrate led to a frequency shift of –183 Hz. By contrast, adsorption on the 1k mPEG-SH-functionalized gold surface was –7 Hz, which indicates a 96% reduction on the functionalized surface. With increasing mPEG-SH molecular weight, there was a further decrease in the amount of adsorbed particles, with –2 and –1 Hz shifts for 2k and 5k Da mPEG-SH chains, respectively. These values indicate ≥99% blocking of vesicle adsorption. Taking into account comparable blocking properties and appreciably shorter chain length in order to minimize steric blocking within the nanohole, the 2k Da mPEG-SH chains were selected for further testing.

Virus-like particle adsorption onto nonfunctionalized and functionalized gold nanohole arrays was next investigated while tracking changes in the wavelength position of all three transmission peaks.[51] After establishing a baseline signal in aqueous buffer solution, addition of virus-like particles was initiated at $t = 5$ min under continuous flow conditions and there was a redshift in all three peaks (**Figure 2**a). Monotonic adsorption was observed and the greatest peak shift was recorded for Peak 2 (1.7 nm). Smaller peak shifts of 1.2 and 0.7 nm were observed for Peaks 1 and 3, respectively. The peak shifts likely arise from adsorbed particles on top of the nanoholes as well as inside the holes. A similar experiment was also performed using functionalized gold nanoholes for which the peak shift is attributed to virus-like particles only at the nanohole positions (Figure 2b). In this case, Peak 2 again had the greatest shift (1.0 nm) while the shifts for the other peaks were appreciably smaller (0.3 nm). Of note, Dahlin et al. previously reported that immobilization of zwitterionic

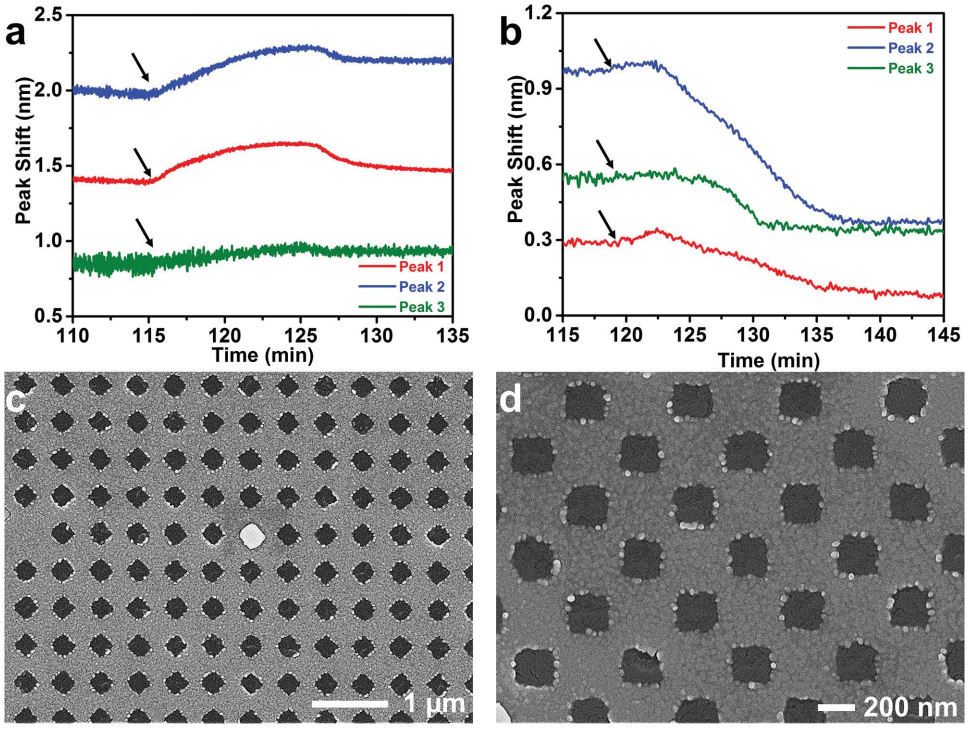

Figure 3. Evaluation of AH peptide-induced rupture of single virus-like particles. Nanohole SPR experiments were performed on a) nonfunctionalized and b) mPEG-SH-functionalized nanohole arrays. Spectral shifts as a function of time were recorded for all three transmission peaks. The baseline signal corresponds to adsorbed virus-like particles after an additional BSA blocking step. Then, 10 μM AH peptide was added (denoted by arrow) and the particle rupture process was tracked. SEM images obtained at c) 20 000× and d) 40 000× magnification show that nearly all virus-like particles were ruptured on the mPEG-SH-functionalized nanohole array.

lipid vesicles (via DNA hybridization) inside randomly distributed gold nanoholes of comparable size leads to a peak shift of 0.3 nm for a sensor system with a 220 nm RIU^{-1} bulk sensitivity.[22] Taken together, the results here demonstrate that the peak shift caused by virus-like particle adsorption is greater on nonfunctionalized surfaces in part because there are a greater number of available adsorption sites. At the same time, the data suggest that virus-like particles selectively adsorb only at the nanohole positions on the functionalized surfaces. Of the three evaluated spectral signatures, the data show that Peak 2 has the highest sensitivity to particle adsorption inside the nanoholes.

To confirm that single virus-like particles are in fact immobilized inside the functionalized nanoholes, SEM experiments were also performed. Virus-like particles were incubated for 3 h with a functionalized nanohole array and then extensively rinsed with buffer solution, followed by sample preparation. The SEM images verified that single particles were immobilized in nanoholes without nonspecific vesicle adsorption on the gold surface (Figure 2c). In a 15 × 20 nanohole array, at least 49% of the nanoholes contained a single virus-like particle while the rest of the nanoholes were empty. Among the nanoholes with virus-like particles, 82% of the particles were mainly inside the nanohole while 18% of the particles were partially inside the nanohole and appeared to protrude. In the latter case, the particles were still exclusively located at the nanohole positions, supporting that the functionalization scheme is selective as there was no particle adsorption onto the other regions of the substrate. Figure 2d presents a magnified view of the nanohole array which depicts all three cases: (i) no vesicle in the nanohole; (ii) one particle predominately on top of the nanohole; and (iii) one particle predominately inside the nanohole. Taken together, the data indicate that single virus-like particles can be immobilized inside the functionalized nanoholes for biosensing applications.

Finally, we examined the AH peptide-induced rupture of adsorbed virus-like particles in the two nanohole configurations. In the nonfunctionalized nanoholes, 10 μM AH peptide addition at t = 115 min induced a redshift in the positions of Peaks 1 and 2 (**Figure 3**a). The magnitude and characteristics of the peak shifts were similar for both transmission peaks. First, there was a moderate increase in the peak position followed by a minor decrease, which resulted in a net redshift. The observation is consistent with peptide binding to the adsorbed particles and induction of a structural transformation.[52,53] Because AH peptide-induced vesicle rupture can promote supported lipid bilayer formation on bare gold substrates,[54] the likely scenario here is that the rupture process leads to lipid bilayer formation on the sidewalls of the nonfunctionalized gold nanoholes. In turn, the lipid mass, on average, will be closer to the plasmonic substrate which leads to the redshift.[29] By contrast, there was negligible change in the position of Peak 3 which supports that this transmission peak is more sensitive to the local refractive index around the rim of the nanohole rather than that inside the nanohole.

When 10 μM AH peptide was added at t = 120 min to the adsorbed virus-like particles in the functionalized nanoholes,

remarkably different responses were observed (Figure 3b). Initially, there was a transient 3 min period of minimal response followed by a significant blueshift in all three peak positions. As with particle adsorption (cf. Figure 2b), the greatest shift was again recorded for Peak 2, with a decrease of 0.5 nm. In addition, the shifts recorded for Peaks 1 and 3 had similar magnitudes, with decreases around 0.2 nm. Hence, while Peak 1 has the greatest bulk refractive index sensitivity, Peak 2 was the most sensitive position to follow virus-like particle adsorption and peptide-induced rupture. In order to confirm AH peptide-induced particle rupture in the functionalized nanohole array, SEM experiments were performed. A similar procedure was used as described above, albeit with two additional steps. After virus-like particle incubation and rinsing, the nanoholes were again incubated in an AH peptide solution for 2 h, followed by another round of rinsing and sample preparation. Figure 3c demonstrates nearly complete particle rupture (>99%) in a 9×12 nanohole array. A magnified view of the nanohole array further supports this observation, with no evidence of particles in nanoholes (Figure 3d). To explain why there is a net blueshift in the nanoplasmonic response, we may recall that the sidewalls of functionalized nanoholes are resistant to bilayer formation, which represents an important sensing advantage over existing nanoparticle-based systems which report a negligible shift or a redshift.[55] When a lipid vesicle or virus ruptures, there is a net loss of lipid mass from the nanohole which is consistent with the experimentally observed blueshift and offers a biologically relevant measurement readout.

Taken together, the findings in this study outline a biosensing scheme to immobilize and characterize single lipid vesicles and virus particles in functionalized nanoholes. It was determined that the optical transmission peaks are sensitive to different regions of the sensing volume, and detailed characterization of the different peaks allowed us to identify optimal sensing strategies for bulk versus local refractive index sensitive measurements. Here, we explored these features in the context of AH peptide-induced virus-like particle rupture which is analogous to the peptide-mediated rupture of dengue virus particles as observed by nanoparticle tracking analysis. Like other single-vesicle surface measurements, our approach has a key advantage over solution measurements that vesicle-peptide interactions can be tracked without effects of vesicle–vesicle interactions. Furthermore, we observe that the functionalized nanoholes resist lipid bilayer formation on the sidewalls after particle rupture, which enables more accurate profiling of the rupture process. Compared to other single particle immobilization approaches based on tethering randomly arranged lipid vesicles to biotin-functionalized surfaces,[56] our approach is label-free and does not require specific attachment chemistries. Instead, it relies on selective, passive adsorption based on a generic surface functionalization scheme, and is amenable to nanoscale and mesoscale biological particulates in general. The features of the nanohole array can be easily customized in order to control the size of deposited biomacromolecules. In future work, it would be interesting to take advantage of temperature-dependent nanoplasmonic biosensing[57] in order to investigate the effects of virus particle conformation (see, e.g., Zhang et al.[58]) on the activity of virucidal drugs. Going beyond particle detection and receptor–ligand interactions, this study opens the door to new possibilities for nanohole biosensing applications involving lipid vesicles and other macromolecular assemblies such as viruses and exosomes.

Experimental Section

Fabrication of Periodic Nanohole Array: A Si template patterned with a square array of deep circular trenches (200 nm in diameter, 500 nm in period, and 600 nm in depth) was fabricated using nanoimprint lithography (Nanonex, NX-B200) and deep reactive ion etching (Plasma-Therm, Apex SLR-770). A 200 nm thick layer of Au was then deposited on the Si template (Forrotec, Temescal VES 2550), creating a metal nanohole array naturally on top of the deep circular trench array. Finally, the Au nanohole array generated on the Si template was peeled off by template-stripping with optical epoxy (Norland, NOA 61) and transferred to a glass substrate.

Surface Functionalization: In order to block virus-like particle adsorption onto gold surfaces, a pretreatment step was carried out whereby thiol-terminated methoxy polyethylene(glycol) (mPEG-SH) (Creative PEGworks, Chapel Hill, NC) was covalently attached to the gold surface. First, a gold surface was rinsed with MilliQ-treated water and ethanol, followed by air drying and treatment with UV/ozone cleaning (PSD-UV, Novascan Technologies Inc., IA, USA) for 10 min. The treated gold surface was then incubated overnight in 2 mg mL^{-1} mPEG-SH in 10 mM Tris buffer solution [pH 8] and extensively rinsed with water before experiment. 2 kDa mPEG-SH was used for all nanohole SPR experiments and 1, 2, or 5 kDa mPEG-SH was used in the QCM-D experiments. Nonfunctionalized gold nanohole arrays were cleaned with water and ethanol, followed by air drying and treatment with UV/ozone cleaning for 5 min before experiment.

Model Virus Particle Preparation: Cholesterol-enriched model virus particles were prepared by the thin film hydration and extrusion method. 1,2-dioleoyl-*sn*-glycero-3-phosphocholine (DOPC) and cholesterol (Chol; ovine wool, >98%) were purchased from Avanti Polar Lipids (Alabaster, AL, USA). DOPC was supplied in chloroform, and Chol was obtained in dry powder form and subsequently solubilized in chloroform with a trace amount of methanol. After mixing DOPC and Chol to the desired molar ratio (70 mol% DOPC and 30 mol% Chol), thin films were prepared by first drying the reagents in chloroform under a gentle stream of nitrogen air at room temperature. After overnight storage in a vacuum desiccator, the dried lipid films were hydrated in aqueous buffer solution at a lipid concentration of 5 mg mL^{-1} and the solution was subjected to vortexing. The resulting multilamellar vesicles were extruded by using a Mini Extruder (Avanti Polar Lipids) through a polycarbonate membrane with 100 nm diameter pores and then again through a polycarbonate membrane with 50 nm diameter pores, and finally through a polycarbonate membrane with 30 nm diameter pores. The resulting virus-like particle solutions were diluted before experiment, and were used within 3 d of preparation. The aqueous buffer solution used in all experiments was 150 mM NaCl and 10 mM Tris [pH 7.5]. All buffers and solutions were prepared with 18.2 MΩ cm MilliQ-treated water (MilliPore, Billerica, MA). The average diameter of the extruded particles was ≈75 nm, as

measured by dynamic light scattering measurements with a 90Plus particle size analyzer (Brookhaven Instruments, NY, USA).

Peptide Reagent: High purity AH peptide (>95%) was synthesized by Anaspec Corporation (San Jose, CA, USA). The sequence of the AH peptide is H-Ser-Gly-Ser-Trp-Leu-Arg-Asp-Val-Trp-Asp-Trp-Ile-Cys-Thr-Val-Leu-Thr-Asp-Phe-Lys-Thr-Trp-Leu-Gln-Ser-Lys-Leu-Asp-Tyr-Lys-Asp-NH_2. The as-supplied lyophilized form was initially solubilized in DMSO and then diluted in water in order to prepare a stock concentration of 2 mg mL^{-1} peptide (8% v/v DMSO). The exact molar concentration of peptide in solution was determined by standard absorbance measurements at 280 nm. For experiment, the peptide stocks were diluted accordingly with aqueous buffer solution [10 mM Tris (pH 7.5) and 150 mM NaCl] and the final DMSO concentration was less than 0.3% v/v.

Quartz Crystal Microbalance-Dissipation Measurements: QCM-D experiments were performed on a Q-Sense E4 instrument (Q-Sense AB, Gothenburg, Sweden). Experimental data were collected at several overtones and the changes in frequency (Δf) and energy dissipation (ΔD) were monitored as functions of time. The reported measurement values are from the third overtone ($n = 3$) and were normalized accordingly ($\Delta f_{n=3}/3$). All measurements were performed on QCM-D sensor crystals (Q-Sense AB) with gold surface coating. The substrates were cleaned with 1% w/w sodium dodecyl sulfate (SDS) solution, and then sequentially rinsed with water and ethanol. After gentle drying with a stream of nitrogen air, the crystals were subjected to oxygen plasma treatment (Harrick Plasma, Ithaca, NY, USA) at maximum radiofrequency for 1 min immediately before experiment.

Nanohole Surface Plasmon Resonance Measurements: Extinction measurements were performed in optical transmission mode using the Insplorion XNano instrument (Insplorion AB, Gothenburg, Sweden). Bulk refractive index sensitivity measurements were conducted on nonfunctionalized gold nanohole arrays by adding glycerol–water mixtures with increasing glycerol fractions (0–35 wt%) and recording the spectral shift for each transmission peak. For experiments on functionalized nanohole arrays, the nanoholes were precoated with mPEG-SH and the baseline signal was recorded in aqueous buffer solution. Then, a 0.3 mg mL^{-1} virus-like particle solution was added until the adsorption process reached saturation. Next, 50 μM bovine serum albumin (BSA) was added in a blocking step followed by buffer rinse. Finally, 10 μM AH peptide was added in order to induce particle rupture. All reagents were introduced under continuous flow at a rate of 41.8 μL min^{-1} as controlled by a peristaltic pump (Reglo Digital, Ismatec, Glattbrugg, Switzerland). Data processing was performed using the Insplorer software (Insplorion AB) and a custom MATLAB script was used to fit a polynomial function to the peaks in the transmission spectrum in order to calculate the peak positions as a function of time.

Scanning Electron Microscopy Imaging: Functionalized gold nanohole arrays were incubated with 0.3 mg mL^{-1} virus-like particle solution for 4 h followed by extensive rinsing with MilliQ-treated water. In some cases, there was an additional incubation step with 52 μM AH peptide, followed by another round of rinsing. After vesicle and/or peptide treatment was complete, the samples were incubated in a 2% v/v aqueous glutaraldehyde solution, followed by water rinsing. The samples were extensively dried, and then coated with a 10 nm thick layer of gold with a JFC-1600 sputter coater (Auto Fine Coater, JEOL, Tokyo, Japan) (20 mA, 60 sec). SEM imaging was performed using a FESEM 7600F instrument (JEOL, Japan) with an acceleration voltage of 5 kV at different magnifications.

Nanoparticle Tracking Analysis: Nanoparticle tracking analysis experiments were conducted with a Nanosight LM10 instrument (Malvern Instruments, Malvern, UK) in order to measure the size distribution of dengue virus particles (type 2, New Guinea C strain) before and after treatment with 26 μM AH peptide at 37 °C for 1 h. A 405 nm laser source was used to illuminate virus particles within the laser beam in order to cause Rayleigh scattering and scattered light from individual particles was visualized by optical microscope (20× magnification). The time-resolved Brownian motion of individual particles was recorded by camera for a time period of 3 min at a rate of 25 frames per second, leading to calculation of the hydrodynamic diameter of individual particles by the 2D Stokes–Einstein equation.[59] Video capture and data analysis parameters were controlled using the NTA 3.1 software program. Before experiment, the dengue virus specimen was propagated in C6/36 cells, irradiated with ultraviolet light for 30 min, and supplied in DMEM culture supernatant at an estimated concentration of 10^5 plaque forming units μL^{-1}.

Acknowledgements

The authors thank Dr. Olof Andersson for assistance with data analysis and Dr. Sven Hobbie for supplying virus reagents. This work was supported by the National Research Foundation grant NRF-NRFF2011–01 (N.-J.C.) and the National Medical Research Council grant NMRC/CBRG/0005/2012 (N.-J.C.). S.H.O. and N.J.W. acknowledge support from the U.S. National Science Foundation (NSF CAREER Award) and the MnDRIVE Research Initiative.

[1] G. Raposo, W. Stoorvogel, *J. Cell Biol.* **2013**, *200*, 373.
[2] S. Stanley, *Curr. Opin. Biotechnol.* **2014**, *28*, 69.
[3] A. S. Fauci, D. M. Morens, *N. Engl. J. Med.* **2012**, *366*, 454.
[4] H. D. Marston, G. K. Folkers, D. M. Morens, A. S. Fauci, *Sci. Transl. Med.* **2014**, *6*, 253ps10.
[5] E. De Clercq, *Curr. Opin. Virol.* **2012**, *2*, 572.
[6] G. Hsiung, *Hsiung's Diagnostic Virology*, 4th ed., Yale University Press, New Haven, CT **1994**, p. 46.
[7] E. De Clercq, *Nat. Rev. Drug Discovery* **2002**, *1*, 13.
[8] V. Lohmann, R. Bartenschlager, *J. Med. Chem.* **2014**, *57*, 1627.
[9] J. A. Jackman, N.-J. Cho, *Biointerphases* **2012**, *7*, 18.
[10] J. N. Anker, W. P. Hall, O. Lyandres, N. C. Shah, J. Zhao, Van R. P. Duyne, *Nat. Mater.* **2008**, *7*, 442.
[11] A. G. Brolo, *Nat. Photonics* **2012**, *6*, 709.
[12] F. Inci, O. Tokel, S. Wang, U. A. Gurkan, S. Tasoglu, D. R. Kuritzkes, U. Demirci, *ACS Nano* **2013**, *7*, 4733.
[13] L. Guo, J. A. Jackman, H.-H. Yang, P. Chen, N.-J. Cho, D.-H. Kim, *Nano Today* **2015**, *10*, 213.
[14] M.-C. Estevez, M. A. Otte, B. Sepulveda, L. M. Lechuga, *Anal. Chim. Acta* **2014**, *806*, 55.
[15] F. Mazzotta, T. W. Johnson, A. B. Dahlin, J. Shaver, S.-H. Oh, F. Höök, *ACS Photonics* **2015**, *2*, 256.
[16] T. W. Ebbesen, H. Lezec, H. Ghaemi, T. Thio, P. Wolff, *Nature* **1998**, *391*, 667.
[17] T. Sannomiya, O. Scholder, K. Jefimovs, C. Hafner, A. B. Dahlin, *Small* **2011**, *7*, 1653.
[18] A. Lesuffleur, H. Im, N. C. Lindquist, S.-H. Oh, *Appl. Phys. Lett.* **2007**, *90*, 243110.

[19] A. B. Dahlin, J. O. Tegenfeldt, F. Höök, *Anal. Chem.* **2006**, *78*, 4416.
[20] H. Im, S. H. Lee, N. J. Wittenberg, T. W. Johnson, N. C. Lindquist, P. Nagpal, D. J. Norris, S.-H. Oh, *ACS Nano* **2011**, *5*, 6244.
[21] N. J. Wittenberg, H. Im, X. Xu, B. Wootla, J. Watzlawik, A. E. Warrington, M. Rodriguez, S.-H. Oh, *Anal. Chem.* **2012**, *84*, 6031.
[22] A. B. Dahlin, M. P. Jonsson, F. Höök, *Adv. Mater.* **2008**, *20*, 1436.
[23] H. Im, N. J. Wittenberg, A. Lesuffleur, N. C. Lindquist, S.-H. Oh, *Chem. Sci.* **2010**, *1*, 688.
[24] A. Dahlin, M. Zäch, T. Rindzevicius, M. Käll, D. S. Sutherland, F. Höök, *J. Am. Chem. Soc.* **2005**, *127*, 5043.
[25] C. Escobedo, Y.-W. Chou, M. Rahman, X. Duan, R. Gordon, D. Sinton, A. G. Brolo, J. Ferreira, *Analyst* **2013**, *138*, 1450.
[26] A. A. Yanik, M. Huang, O. Kamohara, A. Artar, T. W. Geisbert, J. H. Connor, H. Altug, *Nano Lett.* **2010**, *10*, 4962.
[27] H. Im, H. Shao, Y. I. Park, V. M. Peterson, C. M. Castro, R. Weissleder, H. Lee, *Nat. Biotechnol.* **2014**, *32*, 490.
[28] W. P. Hall, J. Modica, J. Anker, Y. Lin, M. Mrksich, Van R. P. Duyne, *Nano Lett.* **2011**, *11*, 1098.
[29] M. P. Jonsson, P. Jönsson, A. B. Dahlin, F. Höök, *Nano Lett.* **2007**, *7*, 3462.
[30] F. Eftekhari, C. Escobedo, J. Ferreira, X. Duan, E. M. Girotto, A. G. Brolo, R. Gordon, D. Sinton, *Anal. Chem.* **2009**, *81*, 4308.
[31] C. Escobedo, A. G. Brolo, R. Gordon, D. Sinton, *Anal. Chem.* **2010**, *82*, 10015.
[32] M. Huang, B. C. Galarreta, A. E. Cetin, H. Altug, *Lab Chip* **2013**, *13*, 4841.
[33] S. Kumar, N. J. Wittenberg, S.-H. Oh, *Anal. Chem.* **2013**, *85*, 971.
[34] A. E. Cetin, A. F. Coskun, B. C. Galarreta, M. Huang, D. Herman, A. Ozcan, H. Altug, *Light: Sci. Appl.* **2014**, *3*, e122.
[35] A. F. Coskun, A. E. Cetin, B. C. Galarreta, D. A. Alvarez, H. Altug, A. Ozcan, *Sci. Rep.* **2014**, *4*, 6789.
[36] H. Im, J. N. Sutherland, J. A. Maynard, S.-H. Oh, *Anal. Chem.* **2012**, *84*, 1941.
[37] N.-J. Cho, H. Dvory-Sobol, A. Xiong, S.-J. Cho, C. W. Frank, J. S. Glenn, *ACS Chem. Biol.* **2009**, *4*, 1061.
[38] J. A. Jackman, G. H. Zan, V. P. Zhdanov, N.-J. Cho, *J. Phys. Chem. B* **2013**, *117*, 16117.
[39] J. A. Jackman, R. Saravanan, Y. Zhang, S. R. Tabaei, N. J. Cho, *Small* **2015**, *11*, 2372.
[40] J. Wang, K.-W. Liu, S. L. Biswal, *Anal. Chem.* **2014**, *86*, 10084.
[41] M. C. Wolf, A. N. Freiberg, T. Zhang, Z. Akyol-Ataman, A. Grock, P. W. Hong, J. Li, N. F. Watson, A. Q. Fang, H. C. Aguilar, *Proc. Natl. Acad. Sci. USA* **2010**, *107*, 3157.
[42] P. Kramberger, M. Ciringer, A. Štrancar, M. Peterka, *Virology J.* **2012**, *9*, 1.
[43] B. Brügger, B. Glass, P. Haberkant, I. Leibrecht, F. T. Wieland, H.-G. Kräusslich, *Proc. Natl. Acad. Sci. USA* **2006**, *103*, 2641.
[44] L. Kalvodova, J. L. Sampaio, S. Cordo, C. S. Ejsing, A. Shevchenko, K. Simons, *J. Virol.* **2009**, *83*, 7996.
[45] P. Nagpal, N. C. Lindquist, S.-H. Oh, D. J. Norris, *Science* **2009**, *325*, 594.
[46] J.-C. Yang, H. Gao, J. Y. Suh, W. Zhou, M. H. Lee, T. W. Odom, *Nano Lett.* **2010**, *10*, 3173.
[47] S. H. Lee, T. W. Johnson, N. C. Lindquist, H. Im, D. J. Norris, S. H. Oh, *Adv. Funct. Mater.* **2012**, *22*, 4439.
[48] A. G. Brolo, R. Gordon, B. Leathem, K. L. Kavanagh, *Langmuir* **2004**, *20*, 4813.
[49] H. Lee, S. M. Dellatore, W. M. Miller, P. B. Messersmith, *Science* **2007**, *318*, 426.
[50] N.-J. Cho, C. W. Frank, B. Kasemo, F. Höök, *Nat. Protoc.* **2010**, *5*, 1096.
[51] J. A. Jackman, V. P. Zhdanov, N.-J. Cho, *Langmuir* **2014**, *30*, 9494.
[52] N.-J. Cho, K. K. Kanazawa, J. S. Glenn, C. W. Frank, *Anal. Chem.* **2007**, *79*, 7027.
[53] G. J. Hardy, R. Nayak, S. M. Alam, J. G. Shapter, F. Heinrich, S. Zauscher, *J. Mater. Chem.* **2012**, *22*, 19506.
[54] N.-J. Cho, S.-J. Cho, K. H. Cheong, J. S. Glenn, C. W. Frank, *J. Am. Chem. Soc.* **2007**, *129*, 10050.
[55] H. Z. Goh, J. A. Jackman, S.-O. Kim, N.-J. Cho, *Small* **2014**, *10*, 4828.
[56] S. R. Tabaei, M. Rabe, V. P. Zhdanov, N.-J. Cho, F. Höök, *Nano Lett.* **2012**, *12*, 5719.
[57] E. Oh, J. A. Jackman, S. Yorulmaz, V. P. Zhdanov, H. Lee, N.-J. Cho, *Langmuir* **2015**, *31*, 771.
[58] X. Zhang, J. Sheng, P. Plevka, R. J. Kuhn, M. S. Diamond, M. G. Rossmann, *Proc. Natl. Acad. Sci. USA* **2013**, *110*, 6795.
[59] R. A. Dragovic, C. Gardiner, A. S. Brooks, D. S. Tannetta, D. J. Ferguson, P. Hole, B. Carr, C. W. Redman, A. L. Harris, P. J. Dobson, *Nanomed.: Nanotechnol., Biol. Med.* **2011**, *7*, 780.

Received: June 30, 2015
Revised: August 25, 2015
Published online: October 9, 2015